1-1-2019

High-Performance Graphene-Fiber-Based Neural Recording Microelectrodes

Kezhong Wang
University of Wollongong, kw743@uowmail.edu.au

Christopher Frewin
University of Texas

Dorna Esrafilzadeh
University of New South Wales, dornae@uow.edu.au

Changchun Yu
University of Wollongong, cy470@uowmail.edu.au

Caiyun Wang
University of Wollongong, caiyun@uow.edu.au

See next page for additional authors

High-Performance Graphene-Fiber-Based Neural Recording Microelectrodes

Abstract

Fabrication of flexible and free-standing graphene-fiber- (GF-) based microelectrode arrays with a thin platinum coating, acting as a current collector, results in a structure with low impedance, high surface area, and excellent electrochemical properties. This modification results in a strong synergistic effect between these two constituents leading to a robust and superior hybrid material with better performance than either graphene electrodes or Pt electrodes. The low impedance and porous structure of the GF results in an unrivalled charge injection capacity of 10.34 mC cm −2 with the ability to record and detect neuronal activity. Furthermore, the thin Pt layer transfers the collected signals along the microelectrode efficiently. In vivo studies show that microelectrodes implanted in the rat cerebral cortex can detect neuronal activity with remarkably high signal-to-noise ratio (SNR) of 9.2 dB in an area as small as an individual neuron.

Disciplines

Engineering | Physical Sciences and Mathematics

Publication Details

Wang, K., Frewin, C. L., Esrafilzadeh, D., Yu, C., Wang, C., Pancrazio, J. J., Romero-Ortega, M., Jalili, R. & Wallace, G. (2019). High-Performance Graphene-Fiber-Based Neural Recording Microelectrodes. Advanced Materials, 31 (15), 1805867-1-1805867-10.

Authors

Kezhong Wang, Christopher Frewin, Dorna Esrafilzadeh, Changchun Yu, Caiyun Wang, Joseph Pancrazio, Mario I. Romero-Ortega, Rouhollah Jalili, and Gordon G. Wallace

WILEY-VCH

DOI: 10.1002/ ((please add manuscript number))
Article type: Communication

High performance graphene fiber based neural recording microelectrodes

Kezhong Wang, Christopher L. Frewin, Dorna Esrafilzadeh, Changchun YU, Caiyun Wang, Joseph J. Pancrazio, Mario Romero-Ortega, Rouhollah Jalili, Gordon Wallace**

Kezhong Wang, Changchun YU, Dr. Caiyun Wang and Prof. Gordon Wallace
Intelligent Polymer Research Institute
ARC Centre of Excellence for Electromaterials Science
University of Wollongong
NSW 2522, Australia.

Dr. Rouhollah Jalili
School of Science- Physics
RMIT University
Melbourne, VIC 3001, Australia.

Dr. Dorna Esrafilzadeh
School of Engineering
RMIT University
Melbourne, VIC 3001, Australia.

Dr. Mario Romero-Ortega, Dr. Joseph J. Pancrazio, and Dr. Christopher L. Frewin
Department of Bioengineering
University of Texas at Dallas
800 W. Campbell Road
Richardson, Texas, 75080, United States of America.

E-mail: ali.jalili@unsw.edu.au, gwallace@uow.edu.au

Keywords: soft neural microelectrode, graphene fiber, neural stimulation and recording, neural interface, brain-machine interface

Abstract:

Fabrication of flexible and free-standing graphene fiber based microelectrode arrays with a thin platinum coating, as a current collector, results in a structure with low impedance, high surface area and excellent electrochemical properties. This modification results in a strong synergistic effect between these two constituents consequently leading to a robust and superior hybrid material

with better performance compared to either graphene electrode or Pt electrode. Low impedance and porous structure of the graphene fiber results in an unrivalled charge injection capacity of 10.34 mC/cm^2 with ability to record and detect neuronal activity. Then, the thin Pt layer transfers the collected signals along the microelectrode efficiently. *In-vivo* studies show that microelectrodes implanted in the rat cerebral cortex can detect neuronal activity with remarkably high signal-to-noise ratio of 9.2 dB at area as small as an individual neuron.

Introduction

Chronically implantable microelectrodes enable communication between man-made devices and the nervous system.[1] Neural prostheses and therapies based on electrical stimulation or action potential recording, involve electrodes interfaced to central and peripheral nervous systems.[2-4] A functional microelectrode is required to communicate with an individual neuron to record bio-signals, while delivering sufficient amount of electrical charge to depolarize the neural tissue and initiate a response.[5] Despite many significant breakthrough discoveries and technological innovations in this field, the existing microelectrode technologies have met significant challenges and limitations.[1, 2, 6, 7]

An effective bidirectional communication between a machine and nerve system requires access to a low impedance soft microelectrode with a tip size comparable to individual neurons ($D < 50$ μm and geometric surface area < 2000 μm^2).[3, 8, 9] However, the performance of conventional microelectrodes comprised of noble metals (i.e., gold, platinum (Pt) and platinum/iridium) and crystalline silicon is limited due to their high impedance, low charge injection capacity, low surface area and mechanical mismatch between the electrode and surrounding tissue causing scarring and failure of the device.[4, 10] Innovative microelectrode design and replacing

conventional electrode materials with softer electromaterials are becoming one of the main research focuses to address these challenges for chronic use.[6, 7, 11]

Selection of the electrodes material governs the efficacy, performance, reliability and lifetime of neural interfaces.[12, 13] Furthermore, during the stimulation/recording, the electrode must deliver sufficient amount of charge, but not exceed the threshold for triggering electrolysis of the surrounding media.[3, 13, 14] "The low surface area of conventional noble metal-based electrodes intrinsically restricts the charge injection capacity to ~0.05-0.26 mC/cm^2, and results in low signal to noise ratio for neural recording.[13] These limitations have motivated the evaluation of more complex materials in order to increase the surface area that showed increased charge capacity, including nanoporous Pt (3 mC/cm^2),[15] Pt grass (0.3 mC/cm^2),[16] carbon nanotube arrays (1.6 mC/cm^2),[17] carbon nanotube fibers (6.5 mC/cm^2),[3] nanoporous metal oxides (IrOx, 1 mC/cm^2),[18] nanoporous metal nitrides (TiN, 0.7 mC/cm^2)[19], and laser pyrolysed graphene (3.1 mC/cm^2)[20] Coating strategies have also been used to enhanced electrochemical properties and biocompatibility of the metal electrodes. For instance, coating Pt electrodes with titanium nitride (TiN) improves the charge injection capacity up to 0.87 mC/cm^2 over a capacitive mechanism, which is favorable for *in-vivo* studies.[21] Also, coating with activated Iridium oxide (IrOx) further increase in the charge injection capacity to 1-5 mC/cm^2, through a Faradaic mechanism.[22] However, the Faradaic mechanism limits the stability of the electrode and reduces the safety margin for *in-vivo* use.[23] Another successful strategy involves the electrodeposition of conducting polymers onto the electrode which improves charge injection capacity and reduce electrode impedance For example, PEDOT:PSS,[24] PEDOT:pTS,[25] PEDOT:ClO_4,[25] PEDOT:CNT[19, 26] coatings improve the charge injection capacity of Pt electrodes to 2.92, 2.01, 2.09, and 1.25 mC/cm^2, respectively. These modifications also reduced the electrode impedance significantly to

8, 26.5, 203 and 42 MΩ μm^2, compared to Pt (~390 MΩ μm^2), respectively. However, low environmental stability of the conducting polymers and heterogeneous nature of the coated microelectrode may result in delamination and early failure.[27]

In addition, the low impedance and very fine microelectrode must be stiff enough to penetrate the soft nerve tissue, yet flexible or stretchable to minimize mechanical mismatch with the tissue and accommodate for micro movements once implanted.[7, 9, 28] Nanostructured carbonaceous materials including graphene can provide outstanding electrochemical characteristics while enabling flexibility and strength.[29] Nanotubes and graphene microfibers provide excellent electrochemical properties, high surface area, mechanical strength, high flexibility, and biocompatibility, and thus ideal for electrode fabrication.[30] Indeed, carbon nanotube fibers demonstrated significant electrochemical activity, sensitivity, and resistance to biofouling when implanted, compared with metal electrodes and conventional carbon fibers.[2, 3, 31] Even though the neat carbon nanotube based fiber microelectrodes are stable and able to record neural activity for relatively long periods of time, the spinning process is challenging. Furthermore, the high cost for producing super aligned carbon nanotube arrays (dry spinning),[32] as well as the extremely rigorous conditions needed for their manufacturing including high temperature (> 1000 ° C), and the use of corrosive solvents (e.g. fuming sulfuric acid and chlorosulphonic acid), drastically limits the production of carbon nanotube-based microfibers.[33] In contrast, manufacturing long, neat and flexible graphene microfibers from liquid crystalline dispersions of graphene oxide (LCGO),[34] is simple and cost effective. Furthermore, graphene microfibers have unique mechanical and electrochemical properties in addition to its natural biocompatibility.[35]

The major drawback of free-standing carbon nanotubes and graphene microfibers lies in the high resistivity compared with their metallic counterparts.[36] When a microelectrode is longer than a

few millimetres, the resistivity increases significantly, which poses a significant challenge to low noise recording. In this work, we overcome this limitation by applying a thin coating of Pt (in the range of 200 nm) as the current collector on the wet-spun graphene microfibers. This modification integrates the electrochemical characteristics of graphene and electronic properties of Pt to the microelectrodes, without limiting its mechanical flexibility and high surface area. The low impedance and porous structure of graphene microfibers result in an unrivalled charge injection capacity with the ability to record and detect neuronal activity at much smaller area than the existing technologies. Then, the thin Pt layer transfers the recorded signals along the microelectrode efficiently (Schematic 1).

Results and discussions

Self-assembly of graphene microfibers

The high mechanical strength and super flexibility of graphene oxide sheets allowed direct processing of three-dimensional (3D) structures without the need of any binder to aid the processing.[37] To achieve self-assembled, binder-free, aligned microfibers with reduced graphene sheets,[38] wet-spinning of liquid crystalline dispersions of graphene oxide (LCGO) was conducted using a coagulation bath containing hypophosphorous acid. This coagulation bath reduced the GO during the spinning process without compromising the flexibility and mechanical strength. Flexibility of a microfiber is an important characteristic for fabricating implantable microelectrode, as it minimizes foreign body reaction and maximizes greater proximal neuron survival in comparison with traditional metal electrodes.[39] Flexibility of these graphene microfibers was demonstrated by tying an overhand knot (Figure 1a). Apparent diameter (diameter of a circle with diameter equal to the longest width of the irregular fiber, see Figure S8) of the microfibers was controlled, ranging from 20±3 μm to 40±5 μm, by using 19-23 gauge nozzles,

respectively (Figure 1b-c). Comparison between the cross-sections of these microfibers suggests that those with larger diameters tend to form more irregular shapes with intersheet spaces after drying (Figure 1b and S1). This potentially is due to a more severe shrinkage during the drying process, which in turn, could explain the higher conductivity of the 20±3 μm fibers (205±16 S/cm) compared with 52±0.3 S/cm for the 40±5 μm. Higher magnification SEM image of the cross-section of a typical microfiber presented in Figure 1d shows a particularly aligned feature of the graphene sheets. Here, the *in-situ* reduction of fully ordered GO sheets in liquid crystalline state inhibited the randomization of the morphology by preventing the relaxation phase. In fact, the inherent LC order was maintained and allowed the aligned assembly of GO microfibers. Furthermore, the *in-situ* reduction constrained any uncontrolled re-stacking of the sheets. Consequently, a fully ordered and porous architecture was obtained. Such reduced graphene microfibers provided an extremely high surface area of up to ~2210 m^2 g^{-1} that facilitated the accessibility of electrolyte and ionic diffusion into the resultant electrode.[40]

The electric resistance of these microfibers was affected by their length, which increased from ~2 to 20 kΩ as the length increased from ~0.5 to 5 cm (Figure 1e). To minimize the effect of the microfiber length on the resistivity and facilitate the recording of fine nerve's signals, one side of the microfibers was sputter coated with up to ~200 nm thick layer of Pt (denoted as GF-Pt). The Pt coating resulted in a significant increase in the conductivity from 205±16 S/cm to 460±30.3 S/cm (Figure S2). Moreover, as Pt acts as current collector, the increase in the resistivity due to the length of microfibers became considerably less detrimental (Figure 1e). Minimization of the resistivity is particularly desirable to achieve noise reduction, stability of recordings and effective electrical stimulation.

Microelectrode fabrication

Microelectrodes were fabricated by insulating each individual platinized microfiber with an insulating polymer coating of ~2 μm (parylene-C, denoted as GF-Pt-PC-20/40), before a sharp cut of the tip in a liquid nitrogen bath; leaving only the tip exposed as an electrochemically active site. Parylene-C was selected due to its high dielectric property, biocompatibility, pin-hole free and uniform coatings, and its common use for neural prostheses. [41] Microelectrodes made from bare graphene microfiber (i.e., no Pt coating) were fabricated for comparison (Figure S3). Moreover, while the polymer coating process increased the robustness of the graphene microfibers, the flexibility was also improved as demonstrated by tying an overhand knot (Movie 1 and Figure S4). Figure 1 f-h shows SEM images of a typical microfiber after each coating step. Both Pt and parylene-C coatings formed thin layers around the microfibers, retaining the porous structure and high surface area at the tip, as evidenced by high-resolution SEM microscopy images (Figure 1 i-l). The high surface area should result in high recording sensitivity, and a large charge injection capacity with low impedance at 1 Hz to 10 kHz (see following section).

Electrochemical characterization

During the stimulation and recording of bioelectric actions, the electrode carries out the function of transduction from the ionic currents in the electrolyte into an electric current in the measurement system.[42] High electrical impedance of the interface between electrode and living tissue can negatively impact the signal-to-noise ratio and increase signal distortion. This particularly becomes very important for microelectrodes due to the reduced dimensions. Electrochemical performance of the graphene microelectrodes was evaluated by electrochemical impedance spectroscopy (EIS), cyclic voltammetry (CV), and calculations of charge storage capacity and charge injection limit (Figure 2). An electrode made from Pt wire of similar diameter with microfibers was also fabricated and tested as the control. EIS analysis showed that the impedance

of graphene microelectrodes was ~2 orders of magnitude lower than the Pt electrode in the range of frequencies tested (1 Hz to 10 kHz, Figure 2a). Particularly, the specific impedance at 1 kHz was over 50 times lower than the Pt electrode (GF-20=8.7±1.1MΩ μm^2, GF-40=28.4±4.1 vs Pt~500 MΩ μm^2). This large reduction in the impedance of the graphene microelectrodes was as a result of the increased available surface area of fully ordered and separated graphene sheets. Furthermore, the specific impedance of the Pt modified microelectrodes (at 1 kHz) was ~5 and ~300 times lower than neat graphene and Pt microelectrodes, respectively. Adding a thin layer of Pt on the graphene microfiber (as current collector) resulted in a strong synergistic effect leading to a robust and superior hybrid microelectrode with lower impedance.

At an ideally polarisable electrode during the stimulation, the charge passed would be completely attributed to the capacitance rather than any Faradic reaction.[13] The phase lag of microelectrodes (Figure 2b) indicates that a capacitive charging-discharging process controls the electrochemical interaction at the exposed tip over the double layer of the microelectrode tip (an adsorption controlled process).

Cyclic voltammetry is a simple and fast technique for measuring the capacitance and Faradaic components at an electrode-solution interface. Figure 2c compares cyclic voltammetry (CV) of different electrodes prepared in this study. Although, both graphene-based microelectrodes showed near-rectangular CV curves, the current of the Pt modified microelectrode was significantly higher than other electrodes. This improvement was due to integration of high conductivity of Pt coating coupled with the high surface area of the GO electrode that allows effective diffusion of electrolyte ions, followed by a facile electron transfer via the Pt layer. Furthermore, the cathodic charge storage capacity of the Pt modified GO microelectrode (GF-Pt-

PC-20), calculated from the CV, was 946±140 mC/cm^2 a value of ~3 orders of magnitudes higher than Pt electrode and ~ 2 times higher than the unmodified graphene microfibers.

Charge injection capacity

Electrical stimulation initiates a functional response by depolarizing the membranes of excitable cells, which is achieved by the flow of ionic current between the electrodes.[8] Voltage transient measurements were made to determine the maximum positive and negative polarization values across the electrode-electrolyte interface, and estimate the maximum charge that can be injected in a stimulation pulse without exceeding the water electrolysis limit. The potential is swept over a wide window to obtain the voltage range where the electrode, electrolyte and water are neither oxidised nor reduced.[13] To ensure the safe polarization of the microelectrode during stimulation, a CV of the microelectrode was recorded by sweeping the potential between the voltage limits of -1.6 V to 1.6 V (vs. Ag/AgCl electrode). In biological systems, this potential range is largely determined by the oxidation and reduction of water (water window). The water oxidation and reduction voltages, indicated by a steep increase in the current, define the electrochemical water window. In this work, the water window of graphene-based microelectrodes was found between -1.0 V to 0.9 V (Figure 2d). The upper panel of Figure 2e shows a typical input biphasic current pulse (300 µA and 20 µs delay). The potential excursion response (lower panel) to the current pulse shows an initial, rapid change in potential, known as the access voltage (Va=-1.35 V), due to the ohmic resistance of the electrolyte, followed by a slowly rising polarization voltage (V_p=-0.90 v), which is due to the charging of the electrode/electrolyte interface. The Vp was calculated by subtracting the Va from the maximum negative voltage in the transient (Vt=-2.25 V). The polarization voltage of phase one of the biphasic pulse was used to determine the charge injection limit and obtained by continuously increasing the current amplitude until the polarization voltage

reached 1.0 V. The charge injection capacity was calculated at V_p= 0.90 V, before the water reduction potential (Figure 2e), to be 10.34±1.5 mC/cm^2 and 8.0±1.0 mC/cm^2 for the GF-Pt-PC-20 and GF-Pt-PC-40 electrodes, respectively; a value ~3 orders of magnitudes higher than Pt and ~ 2 times larger than the unmodified graphene microfibers. The charge injection capacity of the modified microelectrodes was significantly higher than all of the best reported electrode materials; including but not limited to Pt, carbon nanotube fibers, conducting polymer coatings, metal nitride and oxides, as presented in Figure 2f and listed in Table 1. We believe that the synergistic effect of the ordered graphene sheets with low electrical resistivity of Pt layer resulted in this remarkable charge injection capacity along with significantly enhanced electrochemical performance.

Durability characterizations

Over time, chronically implanted electrodes are adversely affected by material degradation, and delamination of the insulator coatings such as parylene, which contribute to device failure. The longevity of the modified microelectrodes was tested using cyclic voltammetry in PBS solution. Figure 3a-b show representative SEM images of typical modified microelectrodes before and after 1000 electrochemical cycles, respectively; the electrode tip did not show any noticeable graphene degradation or parylene delamination. Parylene coating often peels off from rigid underlying electrodes such as Pt and silicon.[43] However, here, the strong interfacial adhesion between the parylene and graphene microfibers, along with the flexibility and softness of the underlying microfiber, resulted in a remarkable stability of the parylene coating. Representative extend CVs and pulse tests shown in Figure 3c-d confirm that there was no noticeable change in the electrochemical performance over the prolonged stability test. Furthermore, the stability of graphene microfibers and the microelectrodes were evaluated against repeated bending and prolonged soaking in PBS solution (Figure 3e-h). The graphene microfibers show outstanding

stability over the bending cycle test, as there was neither obvious difference in conductance between straight and bended microfiber electrodes (105.2±2.7 vs 104.4±3.7 S/cm), nor after 200 times bending (105.2±2.7 vs 102.7±2.5 S/cm). Even after soaking in PBS for 2 weeks, only ~8% conductivity loss was observed. The microelectrodes also could maintain 77.6% and 52.2% charge storage capacity after very tough durability and fatigue tests involving consecutive 200 times 360^{o} folding and 2 weeks soaking in PBS, respectively.

Surgical implantation and neural activity recording

To demonstrate proof-of-concept neural recordings *in-vivo*, first a single microelectrode was implanted in the cerebral cortex of adult rats. Cellular-scale microelectrodes (20μm to 40μm) containing fully ordered graphene sheets, provided us with a sufficient mechanical robustness and sharpness to be inserted and precisely positioned to record neural signals for a total of ten minutes. Figure 4a shows an image of the implanted microelectrode (GF-Pt-PC-40), while Figure S6 shows the snapshot of the recording process. The *in-vivo* test using an array of four tip-exposed microelectrodes GF-Pt-PC-40), aligned and glued together at approximately 1 mm between the wire tips (Figure 4b), was also conducted. Before the *in-vivo* tests, CV of each individual microelectrode was recorded (Figure 4c) to confirm a suitable electrochemical performance. While inserting the bundled microelectrodes, only 3 of the 4 single microelectrodes penetrated into the motor cortex. The fourth microelectrode buckled and subsequently did not enter the brain, so it was eliminated from the recording. Of the three penetrating microelectrodes, two showed single unit activity at a bundle depth of 1500 μm measured from the surface of the cortex. Figure 4d shows 10 second excerpts obtained from the two active electrodes, 550 Hz high pass filtered, and placed side-by-side. The single unit waveforms, which are displayed in Figure 4e, were obtained from the first of the two active electrodes. A second single unit (Figure S7), which was obtained

from the second active electrode, had similar shape. The two single units had average amplitudes of -70.2 µV and -54.3 µV, peak-to-peak voltages of 130.5 µV and 89.7 µV, and SNR of 7.10 dB and 4.43 dB.

Additionally, a single modified microelectrode was implanted to a depth of 1500 µm from the cortical surface, and compared with a graphene only microelectrode (non-modified) implanted to a depth of 2000 µm. Signals obtained from the single microelectrodes produced single unit waveforms which were similar in both shape and duration as compared to the bundled microelectrodes shown in Figure 4. The modified microelectrode displayed two single units of -75.2 µV and -69.3 µV amplitudes, peak-to-peak voltages of 183.4 µV and 123.6 µV, and signal-to-noise ratio (SNR) of 9.2 dB and 8.4 dB respectively. All of our GF-Pt microelectrode signals have demonstrated recording signals, which are larger than previously reported.[3, 44] On the other hand, the GF-only microelectrode showed a weaker performance. Although it possessed signal amplitude of -93.9 µV and a peak-to-peak voltage of 146.4 µV, the noise was considerably larger which lead to a reduced SNR of 3.0 dB.

Carbon nanotubes and graphene have been successfully demonstrated as an alternative platform to other conductive materials used as neural implant devices, such as platinum, iridium, titanium nitride, and iridium oxide, for effectively capturing neural signals.[45] In this communication, we have shown the ability of the platinum modified graphene microfibers for single unit recording capability with high signal-to-noise ratio. Additionally, the recorded units captured by these electrodes were not dissimilar to those reported with other small microelectrode platforms.[3, 24] With the encouraging results from this proof-of-concept evaluation, our future work will be focused on demonstrating the chronic activity of the microelectrode, and testing the hypothesis that the coating of platinum on the outer layer of the graphene microfiber synergistically improves the recording reliability of these electrodes.

Conclusions

In this work, we demonstrated fabrication, characterization, and acute *in-vivo* performance of flexible and freestanding microelectrodes made from graphene fibers coated with Pt for neural stimulation and recording applications at much smaller area than the existing technologies. We found that Pt modification modified resulted in superior electrochemical properties; characterized by remarkably lower impedance, higher charge storage and charge injection capacities. Voltage transient analysis confirmed that these microelectrodes have high charge injection capacity of over 10 mC/cm^2. For *in-vivo* applications, a high SNR of 7.10 dB for the microelectrode array and 9.2 dB for a single microelectrode was achieved during neural recording. Pt-coated graphene fibers seem to be an ideal material for developing the next generation neural stimulation and recording microelectrodes with neural-scale size, low impedance, high charge injection capacity, and high flexibility; thus affording closed-loop, bi-directional implantable devices.

Experimental sections

Detailed experimental processes are provided in the supporting information.

Supporting Information

Supporting Information is available from the Wiley Online Library or from the author.

Acknowledgements

The authors thank the Australian National Fabrication Facility (ANNF) and funding from the Australian Research Council Centre of Excellence Scheme (Project CE 140100012). R.J. thanks

the ARC for financial support through a DECRA (DE180100215). The authors acknowledge use of facilities within the UoW Electron Microscopy Centre.

References

[1] B. Gunasekera, T. Saxena, R. Bellamkonda, L. Karumbaiah, ACS Chem. Neurosci. 2015, 6, 68.
[2] F. Vitale, D. G. Vercosa, A. V. Rodriguez, S. S. Pamulapati, F. Seibt, E. Lewis, J. S. Yan, K. Badhiwala, M. Adnan, G. Royer-Carfagni, M. Beierlein, C. Kemere, M. Pasquali, J. T. Robinson, Nano Letters 2018, 18, 326.
[3] F. Vitale, S. R. Summerson, B. Aazhang, C. Kemere, M. Pasquali, ACS Nano 2015, 9, 4465.
[4] J. Rivnay, H. Wang, L. Fenno, K. Deisseroth, G. G. Malliaras, Sci. Adv 2017, 3, e1601649.
[5] S. M. Won, E. Song, J. Zhao, J. Li, J. Rivnay, J. A. Rogers, Adv. Mater. 2018, 30, 1800534.
[6] W. Mian, M. Gujie, S. Di, B. Nicole, H. Daniel, W. T. J., Adv. Funct. Mater. 2018, 28, 1700905.
[7] T. Klas, K. Dion, D. Bernd, S. Flurin, R. A. F., B. György, V. János, Adv. Mater. 2018, 30, 1706520.
[8] S. F. Cogan, Annu. Rev. Biomed. Eng. 2008, 10, 275.
[9] A. L. Charles, F. G. Winthrop, S. Jun, W. P. Ben, V. Flavia, P. Matteo, J. H. Bradley, J. C. Daniel, E. W. Alice, J. G. Timothy, J. neural eng. 2017, 14, 036006.
[10] Y.-t. Kim, M. I. Romero-Ortega, MRS Bulletin 2012, 37, 573; S. F. Cogan, P. R. Troyk, J. Ehrlich, T. D. Plante, IEEE Trans. Biomed. Eng. 2005, 52, 1612; S. Brummer, L. Robblee, F. Hambrecht, Ann. N. Y. Acad. Sci. 1983, 405, 159.
[11] Y. Lee, S. B. Jun, Bio. Eng. Lett. 2014, 4, 120; G. Mehran, K. Erik, H. John, R. Nick, T. Atsunori, C. Daniel, L. S. Heon, S. Jospeh, H. Milan, C. G. Rees, C. B. S., B. David, U. Ilke, M. G. G., C. S. S., G. Vikash, H. Eric, D. S. A., Adv. Funct. Mater. 2018, 28, 1700232; Z. Siwei, T. Peter, G. Jonathan, W. Yu, L. Wenyi, N. Bradley, Y. Burcin, C. Ying, H. Laurel, R. Javier, O. F. G., K. D. L., Adv. Mater. 2018, 1800598.
[12] W. Tong, K. Fox, A. Zamani, A. M. Turnley, K. Ganesan, A. Ahnood, R. Cicione, H. Meffin, S. Prawer, A. Stacey, Biomaterials 2016, 104, 32; J. G. David, G. Kumaravelu, S. Alastair, F. Kate, M. Hamish, P. Steven, J. neural eng. 2012, 9, 016002.
[13] R. H. Alexander, N. Carrie, C. Paul, C. Robert, G. W. Gordon, J. neural eng. 2018, 15, 046015.
[14] A. Weremfo, P. Carter, D. B. Hibbert, C. Zhao, Langmuir 2015, 31, 2593; F. C. Stuart, A. L. Kip, G. W. Cristin, T. Pavel, J. neural eng. 2016, 13, 021001.
[15] S. Park, Y. J. Song, H. Boo, T. D. Chung, J. Phys. Chem. C 2010, 114, 8721.
[16] C. Boehler, T. Stieglitz, M. Asplund, Biomaterials 2015, 67, 346.
[17] K. Wang, H. A. Fishman, H. Dai, J. S. Harris, Nano Lett. 2006, 6, 2043.
[18] S. Wilks, S. Richardson-Burn, J. Hendricks, D. Martin, K. Otto, Front. NeuroEng. 2009, 2, 1.
[19] R. Gerwig, K. Fuchsberger, B. Schroeppel, G. Link, G. Heusel, U. Kraushaar, W. Schuhmann, A. Stett, M. Stelzle, Front. NeuroEng. 2012, 5.
[20] Y. Lu, H. Lyu, A. G. Richardson, T. H. Lucas, D. Kuzum, Sci. Rep. 2016, 6, 33526.
[21] J. D. Weiland, D. J. Anderson, M. S. Humayun, IEEE Trans. Biomed. Eng. 2002, 49, 1574.
[22] S. F. Cogan, A. A. Guzelian, W. F. Agnew, T. G. H. Yuen, D. B. McCreery, J. Neurosci. Methods 2004, 137, 141.
[23] S. Negi, R. Bhandari, L. Rieth, R. Van Wagenen, F. Solzbacher, J. Neurosci. Methods 2010, 186, 8.
[24] S. Venkatraman, J. Hendricks, Z. A. King, A. J. Sereno, S. Richardson-Burns, D. Martin, J. M. Carmena, IEEE Trans. Neural Syst. Rehabil. Eng. 2011, 19, 307.
[25] R. A. Green, R. T. Hassarati, L. Bouchinet, C. S. Lee, G. L. M. Cheong, J. F. Yu, C. W. Dodds, G. J. Suaning, L. A. Poole-Warren, N. H. Lovell, Biomaterials 2012, 33, 5875.

[26] T. D. Y. Kozai, K. Catt, Z. Du, K. Na, O. Srivannavit, R. u. M. Haque, J. Seymour, K. D. Wise, E. Yoon, X. T. Cui, IEEE Trans. Biomed. Eng. 2016, 63, 111.
[27] T. Boretius, M. Schuettler, T. Stieglitz, Artificial Organs 2011, 35, 245; R. A. Green, N. H. Lovell, L. A. Poole-Warren, Acta Biomater. 2010, 6, 63; R. A. Green, N. H. Lovell, G. G. Wallace, L. A. Poole-Warren, Biomaterials 2008, 29, 3393.
[28] D. Qi, Z. Liu, Y. Liu, Y. Jiang, W. R. Leow, M. Pal, S. Pan, H. Yang, Y. Wang, X. Zhang, Adv. Mater. 2017, 29; S. P. Lacour, S. Benmerah, E. Tarte, J. FitzGerald, J. Serra, S. McMahon, J. Fawcett, O. Graudejus, Z. Yu, B. Morrison, Med. Biol. Eng. Comput. 2010, 48, 945.
[29] C. Cheng, S. Li, A. Thomas, N. A. Kotov, R. Haag, Chem. Rev. 2017, 117, 1826; R. Jalili, D. Esrafilzadeh, S. H. Aboutalebi, Y. M. Sabri, A. E. Kandjani, S. K. Bhargava, E. Della Gaspera, T. R. Gengenbach, A. Walker, Y. Chao, C. Wang, H. Alimadadi, D. R. G. Mitchell, D. L. Officer, D. R. MacFarlane, G. G. Wallace, Nature Communications 2018, 9, 5070.
[30] Deshdeepak Sahni, Andrew Jea, Javier A. Mata, Daniela C. Marcano, Ahilan Sivaganesan, Jacob M. Berlin, Claudio E. Tatsui, Zhengzong Sun, Thomas G. Luerssen, S. Meng, Thomas A. Kent, James M. Tour, J. Neurosurg. Pediatrics 2013, 11, 575; C. Chong, Z. Jianguang, L. Shuang, X. Yi, N. Chuanxiong, S. Zhenqiang, C. C. J. Luis, M. Nan, H. Rainer, Adv. Mater. 2018, 30, 1705452.
[31] W. Harreither, R. Trouillon, P. Poulin, W. Neri, A. G. Ewing, G. Safina, Anal. Chem. 2013, 85, 7447; J. Wang, R. P. Deo, P. Poulin, M. Mangey, J. Am. Chem. Soc. 2003, 125, 14706; I. Yoon, K. Hamaguchi, I. V. Borzenets, G. Finkelstein, R. Mooney, B. R. Donald, PLoS One 2013, 8, e65715; H. Zhang, P. R. Patel, Z. Xie, S. D. Swanson, X. Wang, N. A. Kotov, ACS Nano 2013, 7, 7619.
[32] K. Jiang, J. Wang, Q. Li, L. Liu, C. Liu, S. Fan, Adv. Mater. 2011, 23, 1154.
[33] W. Zhou, J. Vavro, C. Guthy, K. I. Winey, J. E. Fischer, L. M. Ericson, S. Ramesh, R. Saini, V. A. Davis, C. Kittrell, M. Pasquali, R. H. Hauge, R. E. Smalley, J. Appl. Phys. 2004, 95, 649; L. Kou, Y. Liu, C. Zhang, L. Shao, Z. Tian, Z. Deng, C. Gao, Nano Mic. Lett. 2017, 9, 51.
[34] K. S. U. Schirmer, D. Esrafilzadeh, B. C. Thompson, A. F. Quigley, R. M. I. Kapsa, G. G. Wallace, J. Mater. Chem. B 2016, 4, 1142.
[35] D. Esrafilzadeh, R. Jalili, E. M. Stewart, S. H. Aboutalebi, J. M. Razal, S. E. Moulton, G. G. Wallace, Adv. Funct. Mater. 2016, 26, 3105.
[36] H. Rho, M. Park, M. Park, J. Park, J. Han, A. Lee, S. Bae, T.-W. Kim, J.-S. Ha, S. M. Kim, D. S. Lee, S. H. Lee, NPG Asia Mater. 2018, 10, 146.
[37] P. Poulin, R. Jalili, W. Neri, F. Nallet, T. Divoux, A. Colin, S. H. Aboutalebi, G. Wallace, C. Zakri, Proc. Natl. Acad. Sci. 2016, 113, 11088.
[38] R. Jalili, S. Aboutalebi, D. Esrafilzadeh, K. Konstantinov, J. Razal, S. Moulton, G. Wallace, Mater. Horiz. 2014, 1, 87; R. Jalili, S. H. Aboutalebi, D. Esrafilzadeh, R. L. Shepherd, J. Chen, S. Aminorroaya-Yamini, K. Konstantinov, A. I. Minett, J. M. Razal, G. G. Wallace, Adv. Funct. Mater. 2013, 23, 5345.
[39] A. P. Kelsey, C. B. Amy, K. S. Wade, R. C. Jeffrey, J. neural eng. 2012, 9, 046020; T. D. Y. Kozai, Z. Gugel, X. Li, P. J. Gilgunn, R. Khilwani, O. B. Ozdoganlar, G. K. Fedder, D. J. Weber, X. T. Cui, Biomaterials 2014, 35, 9255.
[40] S. H. Aboutalebi, R. Jalili, D. Esrafilzadeh, M. Salari, Z. Gholamvand, S. Aminorroaya Yamini, K. Konstantinov, R. L. Shepherd, J. Chen, S. E. Moulton, P. C. Innis, A. I. Minett, J. M. Razal, G. G. Wallace, ACS Nano 2014, 8, 2456.
[41] F. Cortés-Salazar, H. Deng, P. Peljo, C. M. Pereira, K. Kontturi, H. H. Girault, Electrochim. Acta 2013, 110, 22; C. Hassler, R. P. von Metzen, P. Ruther, T. Stieglitz, J. Biomed. Mater. Res. B 2010, 93, 266.
[42] M. B. A. Fontes, J. Phys. Conf. Ser 2013, 421, 012019.
[43] J. C. Barrese, J. Aceros, J. P. Donoghue, J. neural eng. 2016, 13, 026003.
[44] Z. Irwin, K. Schroeder, P. Vu, D. Tat, A. Bullard, S. Woo, I. Sando, M. Urbanchek, P. Cederna, C. Chestek, J. neural eng. 2016, 13, 046007; D.-H. Kim, J. A. Wiler, D. J. Anderson, D. R. Kipke, D. C. Martin, Acta Biomater. 2010, 6, 57.

[45] G. Guitchounts, J. E. Markowitz, W. A. Liberti, T. J. Gardner, J. neural eng. 2013, 10, 046016; T. D. Y. Kozai, N. B. Langhals, P. R. Patel, X. Deng, H. Zhang, K. L. Smith, J. Lahann, N. A. Kotov, D. R. Kipke, Nat. Mater. 2012, 11, 1065.
[46] Y. Lu, T. Li, X. Zhao, M. Li, Y. Cao, H. Yang, Y. Y. Duan, Biomaterials 2010, 31, 5169.

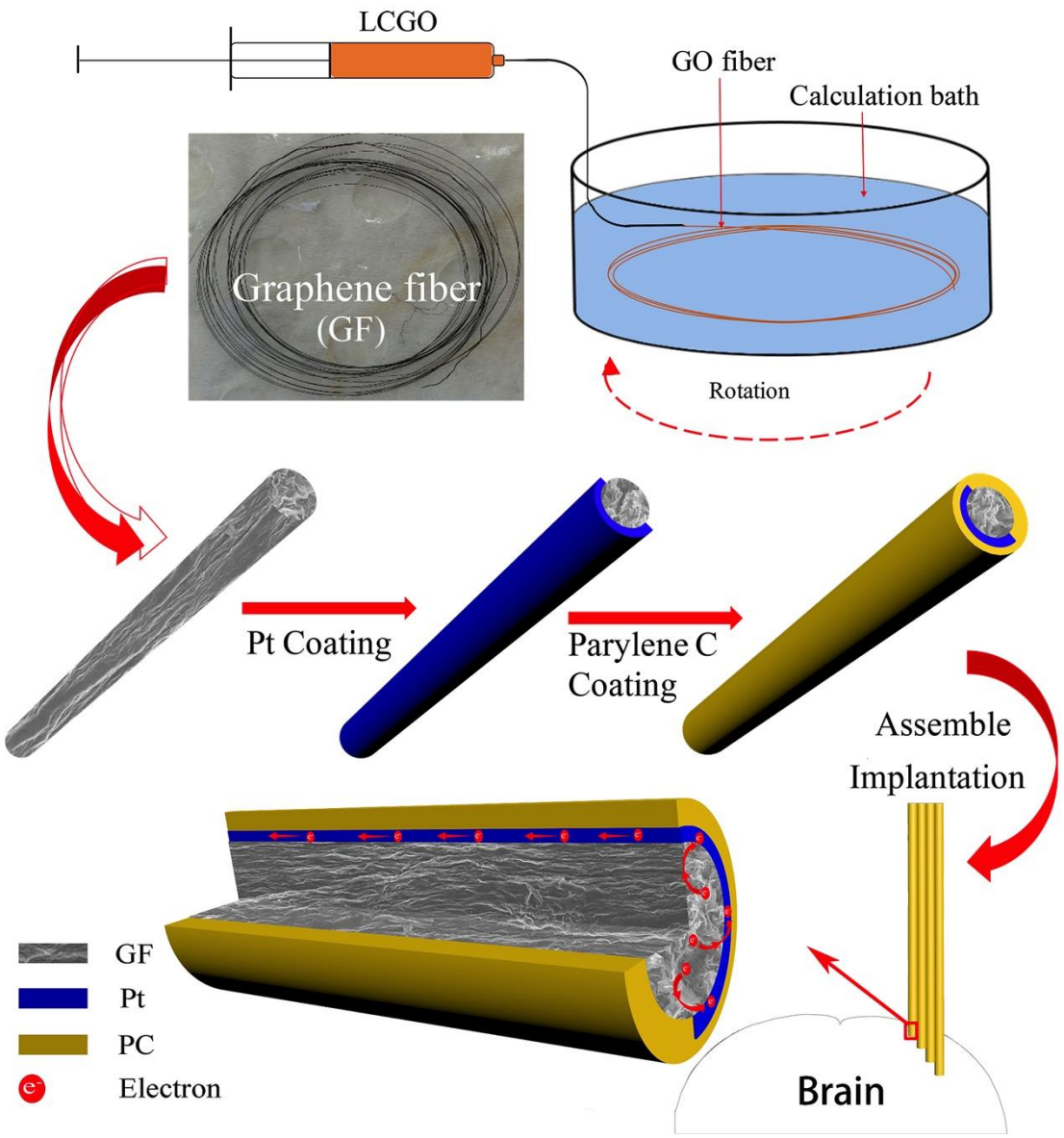

Schematic 1. Process of GO fiber preparation, GF-Pt microelectrode fabrication, and intracortical implantation.

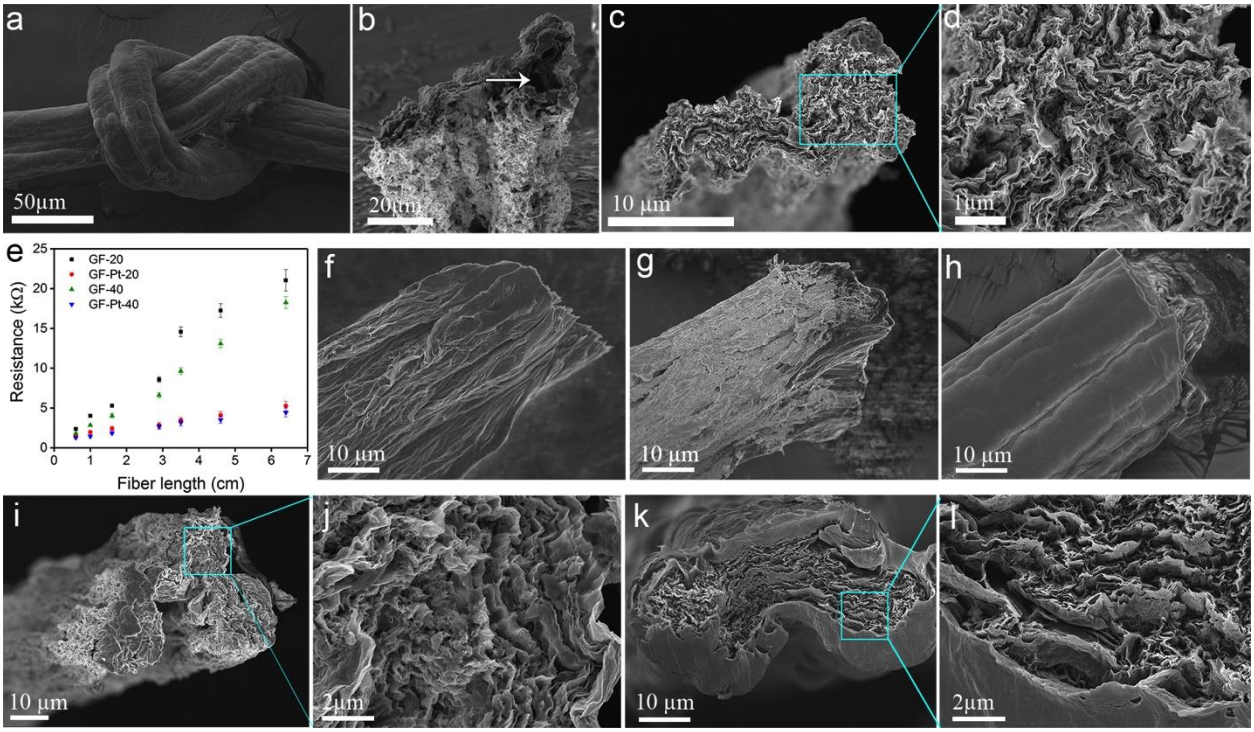

Figure 1. (a) Graphene microfibers shows high flexibility and can be easily tied into a knot; (b-c) SEM images of graphene microfibers with apparent diameter (diameter of a circle with diameter equal to the longest width of the irregular fiber) of (b) 40 µm and (c) 20 µm, respectively. Arrow in (b) shows presence of a void in a typical fiber of larger diameter; (d) Enlarged SEM image of the cross-section shows aligned characteristic features of graphene microfibers; (e) Electrical resistivity of graphene microfibers (D= 20 µm and 40 µm) as function of Pt coating and length; (f-h) SEM images of the outer surface of GF-40, GF-Pt-40, and GF-Pt-PC-40, respectively; (i-j) Cross-section SEM images of GF-Pt-40; (k-l) SEM images of the tip of the final microelectrode (GF-Pt-PC-40).

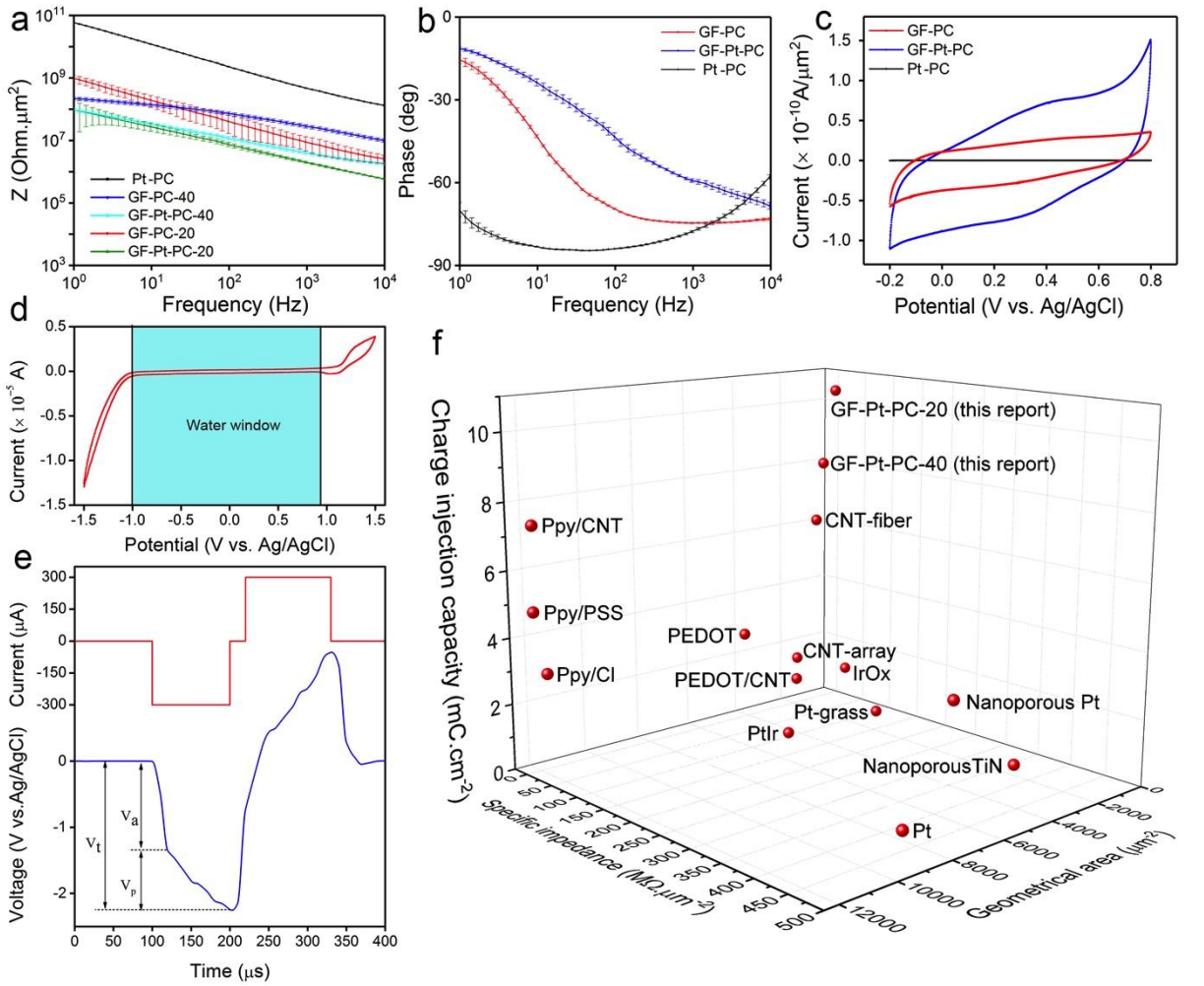

Figure 2. Electrochemical characterization of various microelectrodes made from Pt, graphene microfibers and Pt coated graphene microfibers (D = 20 μm and 40 μm). (a-b) Modulus and phase angle of impedance of microelectrodes, respectively. (c) CVs of the microelectrodes at 10 mV/s in PBS solution. (d-e) Water window and voltage transient test of microelectrodes, respectively. (f) Comparison of the charge injection capacity, specific impedance at 1kHz and geometrical area of the modified microelectrodes with the state-of-art neural interfacing electrodes reported in the literature.

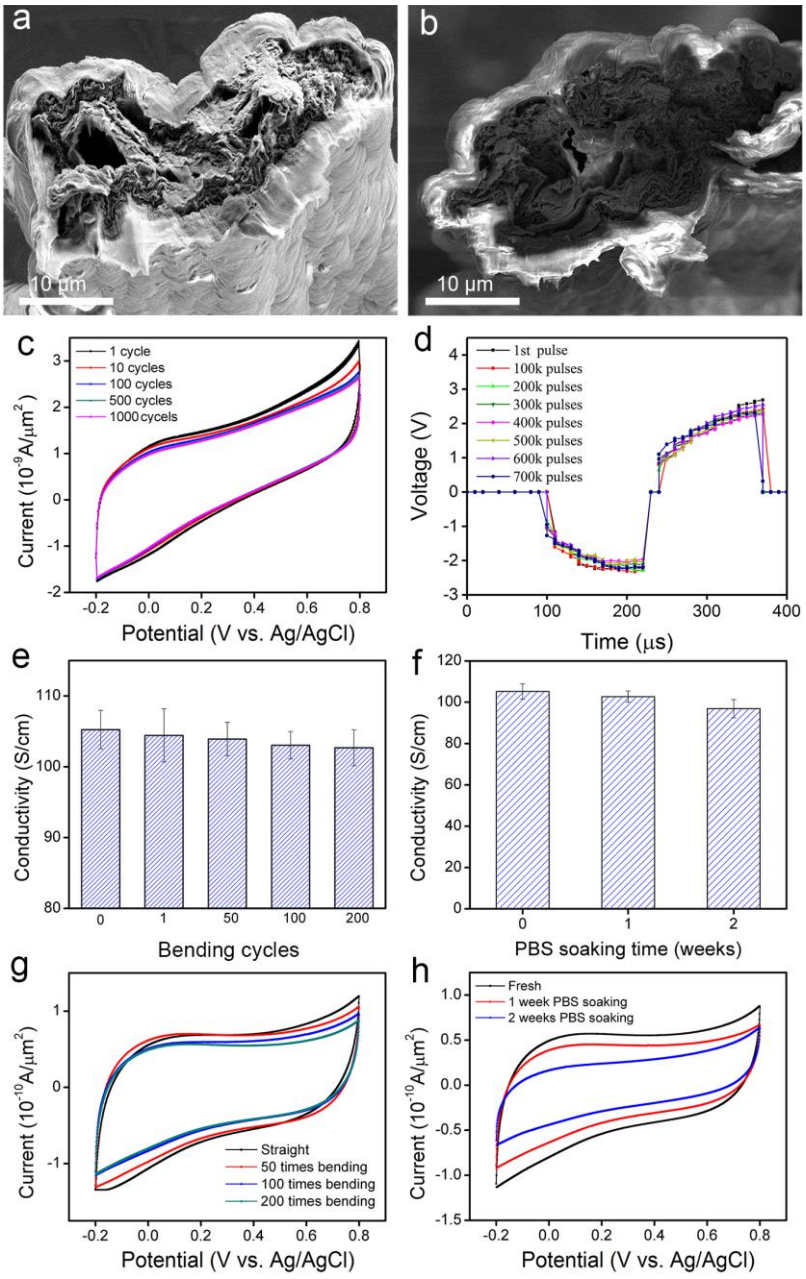

Figure 3. Electrochemical durability characterization of the modified microelectrodes (GF-Pt-PC-40); (a-b) Cross-section SEM image of a typical modified microelectrode (a) before and (b) after 1000 CV cycles at scan rate of 50 mV/s, showing high stability of the microelectrodes. (c) Prolonged CV of the modified microelectrodes, 1000 cycles at scan rate of 50 mV/s. d) Prolonged pulse stability of the modified microelectrodes. (e) Electrical conductivity of the modified graphene microfibers after successive bending cycles, 0 refers to the straight fiber, while 1 refers

to the fiber that was 360° bent. (e-f) Electrical conductivity of the modified graphene microfibers after prolonged PBS soaking; (g-h) CV of the modified microelectrodes after successive bending and prolonged PBS soaking. Number of repeats is 4 independent tests.

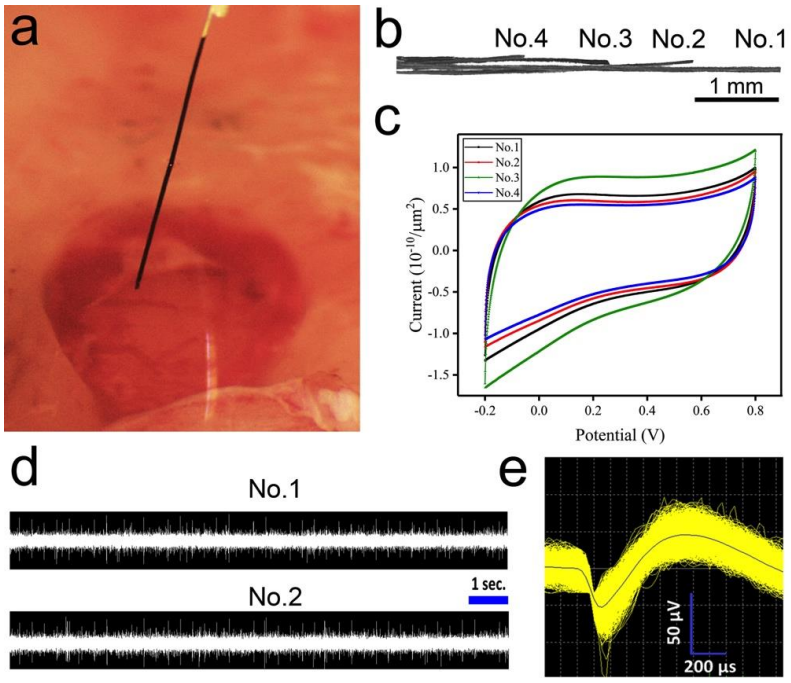

Figure 4. (a) Representative photo of an inserted microelectrode showing the *in-vivo* Cortical Neural Recording (GF-Pt-PC-40). (b) Representative snapshot of the hand assembled microelectrodes array. Microelectrode was assembled from graphene fiber that was coated with Pt and insulated with parylene-C. (c) CV of each individually addressable microelectrodes assembled in one array. All microelectrodes showed very similar electrochemical responses. (d) 10 seconds of 550 Hx high-pass filtered electrical signals obtained from two of the GF-Pt-PC-40 bundled microelectrodes inserted 1.5 mm into the motor cortex of a Long Evans rat at the location of 2.5 mm rostral and 2.5 mm lateral from bregma. (e) 1543 single unit signals obtained over 10 minutes of recording time from one of the GF-Pt-PC-40 implanted microelectrodes. The dark line in the center of the waveforms represents the average single unit signal which has an amplitude of -70.2 µV, and a peak to peak value of 130.5 µV. The units of the second active electrode (not shown), have a similar shape with a slightly lower mean amplitude of -54.3 µV with a peak to peak value of 89.7 µV. The SNR for the two microelectrodes are 7.10 dB and 4.43 dB.

Table 1. Comparison of the electrochemical performance of some of the best performing materials used to fabricate neural interfacing electrodes with the modified microelectrode presented here.

Material	Geometrical surface area (μm^2)	Specific impedance at 1kHz ($M\Omega\ \mu m^2$)	Charge storage capacity (mC/cm^2)	Charge injection capacity (mC/cm^2)	Reference
GF-PC-20	169±25	8.7±1.1	798±110	8.9±1.3	This work (Graphene fiber)
GF-Pt-PC-20		1.9±0.3	946±140	10.5±1.5	
GF-PC-40	749±93	28.4±4.1	200±25	4.7±0.6	
GF-Pt-PC-40		3.9±0.4	361±45	8.0±1.0	
Pt	7,850	424	1.2	0.2	Lu[46]
Nanoporous Pt	5,000	390	~1.2	3	Park[15]

Pt-grass	1,256	125	-	0.3	Boehler[16]
PtIr	4,500	405	8	0.13	Venkatraan[24]
PtIr	17,000	452	1.2	0.15	Vitale [3]
Nanoporous TiN	2,830	155	5	0.7	Gerwig[19]
IrO_x	177	23.54	29	1	Wilks[18]
CNT array	1,962	5.9	-	1-1.6	Wang[17]
CNT fiber	1,450	20.44	372	6.52	Vitale [3]
PPy/Cl	12,240	34.5	495	3.2	Lu[46]
PPy/PSS	12,467	24	705	5	
PPy/CNT	12434	25	1,244	7.5	
PEDOT/PSS	4,500	18	123	2.92	Venkatraan[24]
PEDOT/pTS	-	26.5	402	2.01	Green[25]
PEDOT/ClO_4	-	203	390	2.09	
PEDOT/CNT	2,830	42.45	6	1.25	Gerwig[19]
laser pyrolysis graphene	625,000	324	-	3.1	Lu[20]

The table of contents entry:

Robust, flexible and free-standing graphene fiber based microelectrode arrays with an extremely thin platinum coating demonstrates high performance neural recording microelectrode with low impedance, high surface area, very high charge injection capacity and with unmatched flexibility. *In-vivo* studies show that microelectrodes implanted in the rat cerebral cortex can detect neuronal activity with remarkably high signal-to-noise ratio (SNR) at area as small as an individual neuron.

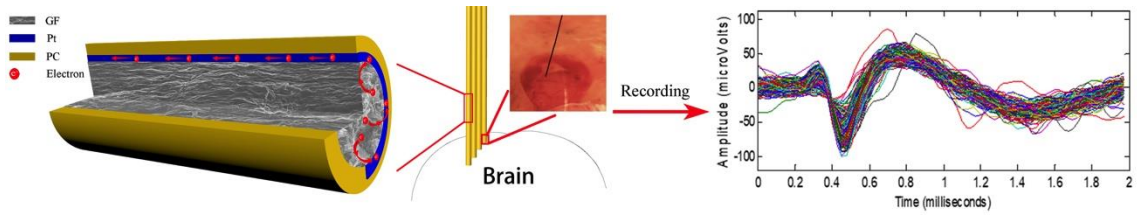

Keyword: soft neural microelectrode, graphene fiber, neural stimulation and recording, neural interface, brain-machine interface

K. Wang, C. L. Frewin, D. Esrafilzadeh, Changchun YU, C. Wang, Joseph J. Pancrazio, M. Romero-Ortega, R. Jalili*, G.G. Wallace*

E-mail: ali.jalili@unsw.edu.au, gwallace@uow.edu.au

WILEY-VCH

Supporting Information

High performance and flexible graphene fiber based neural recording microelectrodes

Kezhong Wang, Christopher L. Frewin, Dorna Esrafilzadeh, Changchun YU, Caiyun Wang, Joseph J. Pancrazio, Mario Romero-Ortega, Rouhollah Jalili, Gordon Wallace**

Kezhong Wang, Changchun YU, Dr. Caiyun Wang and Prof. Gordon Wallace
Intelligent Polymer Research Institute
ARC Centre of Excellence for Electromaterials Science
University of Wollongong
NSW 2522, Australia.

Dr. Rouhollah Jalili
School of Science- Physics
RMIT University
Melbourne, VIC 3001, Australia.

Dr. Dorna Esrafilzadeh
School of Engineering
RMIT University
Melbourne, VIC 3001, Australia.

Dr. Mario Romero-Ortega, Dr. Joseph J. Pancrazio, and Dr. Christopher L. Frewin
Department of Bioengineering
University of Texas at Dallas
800 W. Campbell Road
Richardson, Texas, 75080, United States of America.

E-mail: ali.jalili@unsw.edu.au, gwallace@uow.edu.au

Keywords: soft neural microelectrode, graphene fiber, neural stimulation and recording, neural interface, brain-machine interface

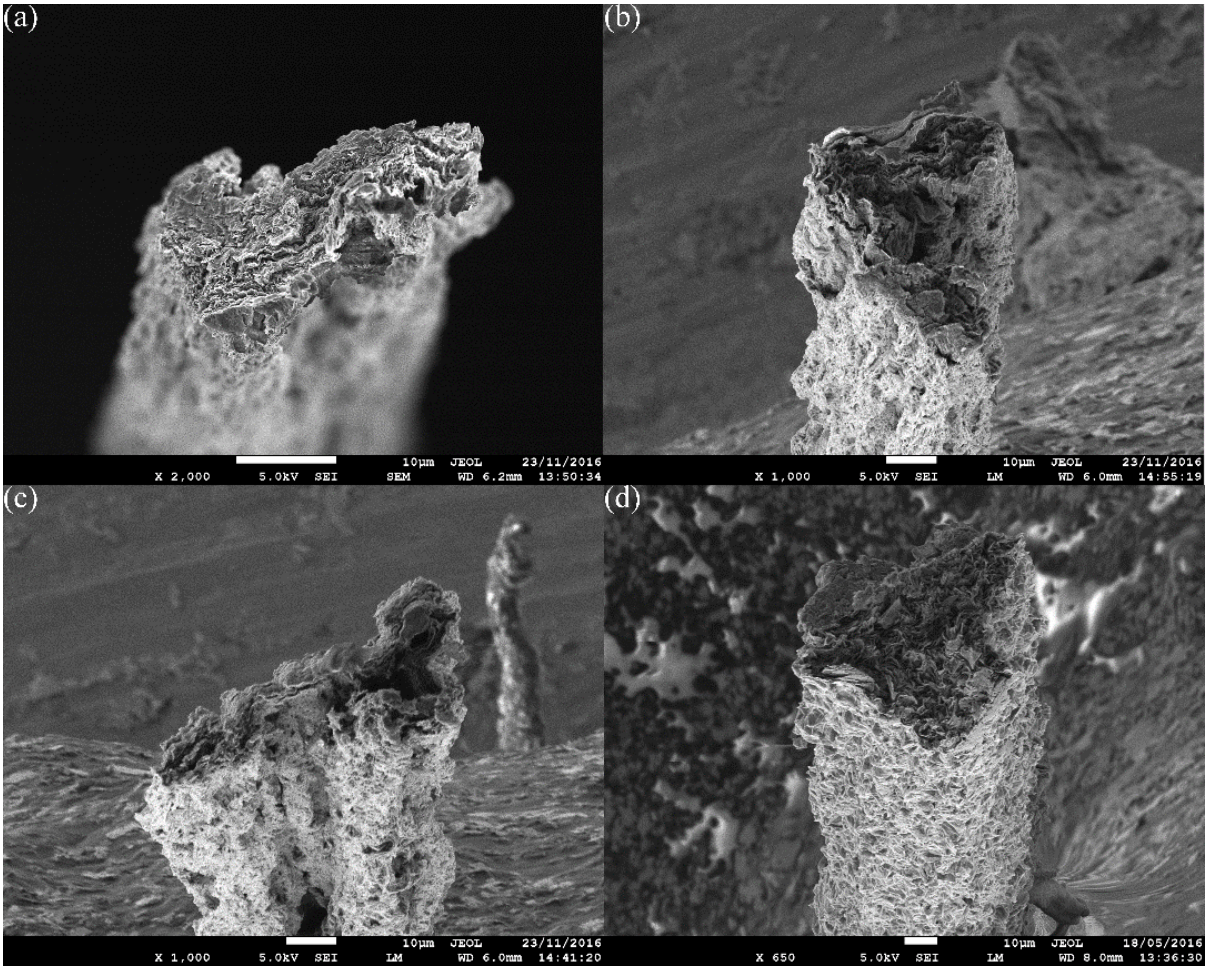

Figure S1. SEM images from the cross-section of various fibers shows that the fibers with larger diameters tend to form some large voids during the drying, due to a larger shrinkage than the smaller fiber.

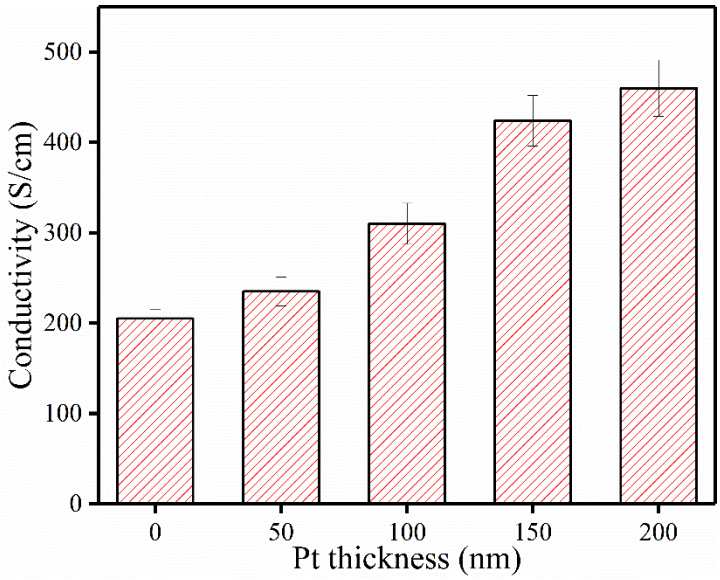

Figure S2. Conductivity of thin graphene fiber with different Pt coating thicknesses.

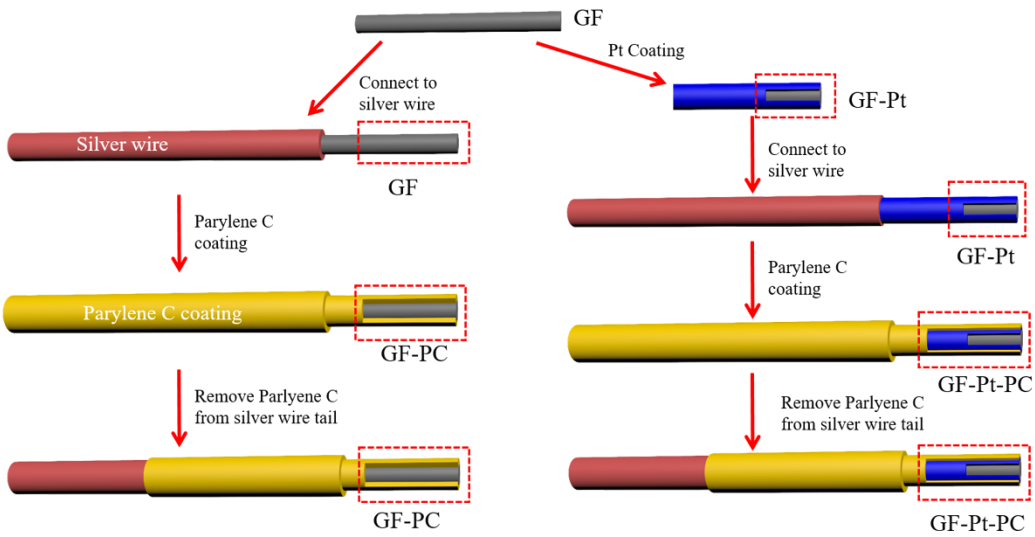

Figure S3. Fabrication of microelectrodes with Pt coating (PF-Pt-PC) and without Pt coating (GF-PC). The tips of each microelectrode are exposed and the parylene C on tails are removed for connection.

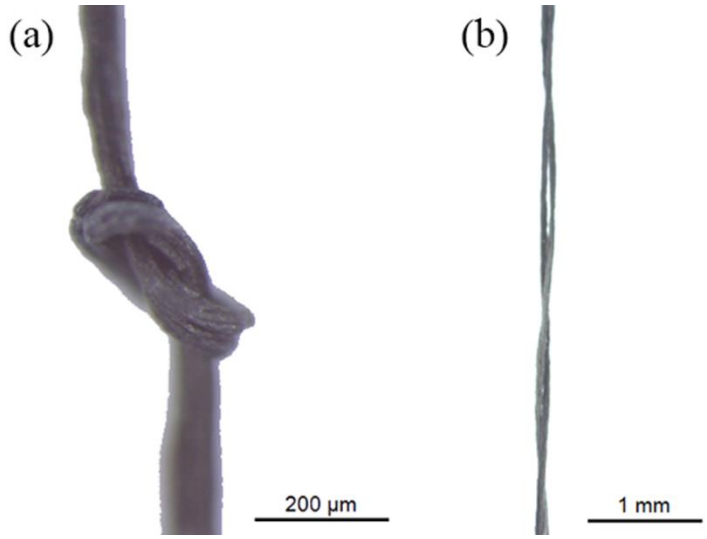

Figure S4. optical microscope images of GF-Pt, which are very flexible and can be easily knotted and twined.

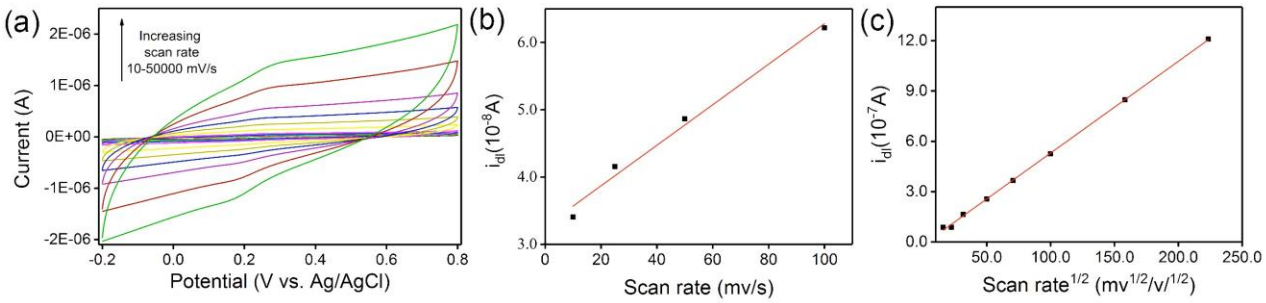

Figure S5. (a) CV measurement of GF-Pt-PC to determine the dynamic behavior over the double layer of graphene. (b) The peak current is linearly dependent on scan rate at low scan rate with linear regression equation as $y=3.2659*10^{-8}+3.0127x$ ($R^2=0.980$), suggesting a surface adsorption-controlled process of GF-Pt-PC. (c) The peak current is linearly dependent on square root of scan rate at high scan rate with linear regression equation as $y=-1.6698*10^{-8}+5.4659x$ ($R^2=0.999$), suggesting a diffusion-controlled process.

Movie 1 A movie showing the process of making knot from a GF-Pt-PC.

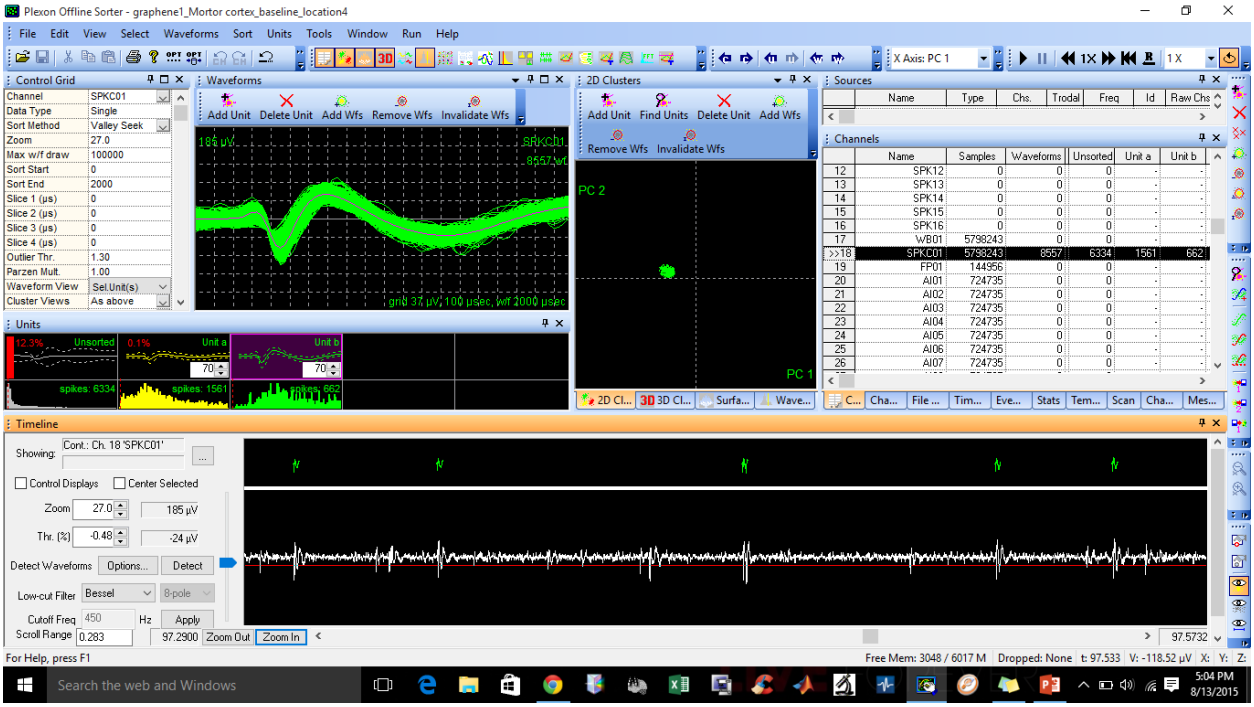

Figure S6. Snapshot of the recording process when a single unit was implanted in the cerebral cortex of adult rats.

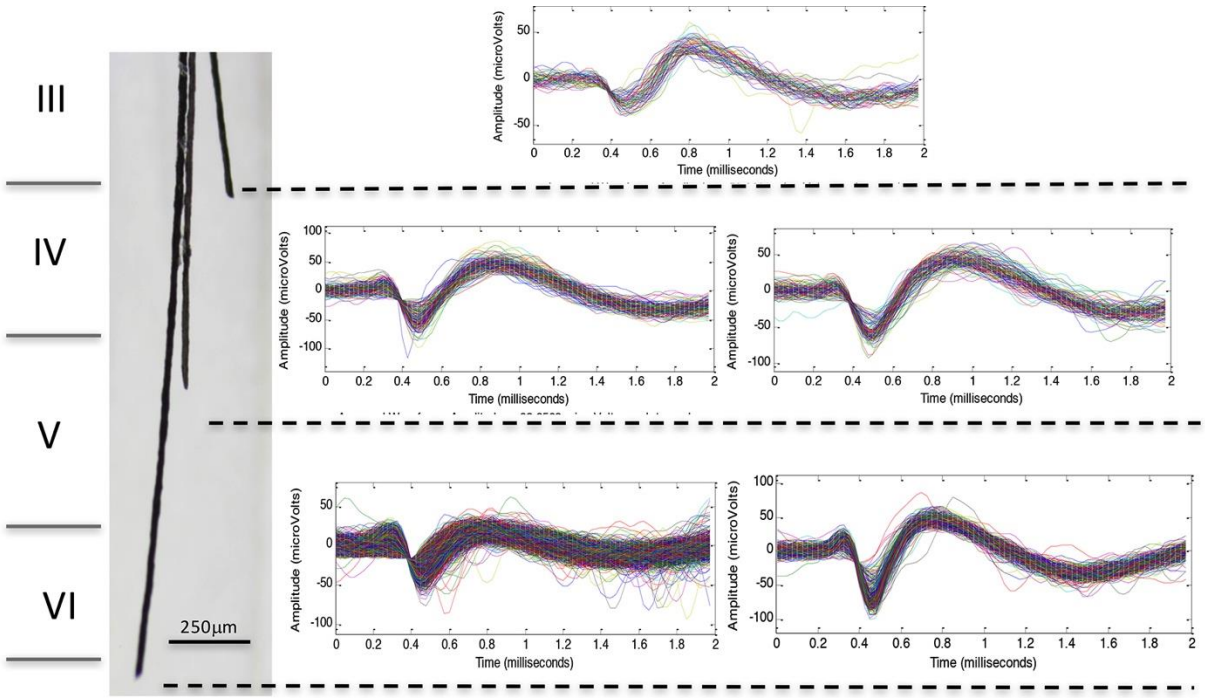

Figure S7. *In-vivo* Cortical Neural Recording using four array electrodes at different depth.

Experimental Section

Microelectrode fabrication and characterization

GFs were fabricated via a wet-spinning process from home-made LCGO, based on our previous work[1]. The fabricated wet LCGO fibers were reduced with hypophosphorous acid solution (50% in water, Sigma-Aldrich) at 80 °C for 24 h. The dried individual GF filaments (40 µm diameter) were deposited with a 200 nm Pt layer by using a sputter coater to make GF-Pts. Thickness of the Pt coating was limited by the recommended coating time of the spotter-coating machine. The 200 nm coating was achieved after 30 min of coating, which was the highest recommended coating time to avoid overheating of the chamber. Therefore, we did not prepared samples with thicker coatings than 200 nm.

The prepared GF-Pts were cut into 8-12 mm pieces and attached to silver wires using conductive silver paint (SPI supplies, Z05002-AB). Then the GF-Pts along with silver wires were coated with Parylene C using a parylene deposition system coater (Specialty Coating System, PDS 2010 Labcoater). The assembled GF-Pt-PCs were dipped into liquid nitrogen for about 10 min and cutting its tip with a sharp scissors exposed the active sites of a microelectrode. The Parlyene C on the tail of the silver wire was removed before test to make it conductive. Electrical conductivity of fibers was measured using a home-made four-point probe conductivity set-up with 240 um probe spacing using a galvanostat current source (Princeton Applied Research 363) and a digital multimeter (Agilent 34401A)[2]. As-prepared fibers and electrodes were directly examined by scanning electron microscopy (JEOL JSM-7500FA) and video microscope (Leica M2056A).

As the cross-section of the fibers are not perfectly circular, we reported the apparent diameter (i.e 20 um) based on the diameter of a circle with a diameter equal to the longest width of the irregular fiber (green circle in the figure S8). However, to have an accurate calculation of the electrode performance, we have measured the actual area using SEM images and ImageJ software (the actual

area is defined with the red line Figure S8). The diameter and the area were measured for 4 samples for each diameter then average and deviation are reported.

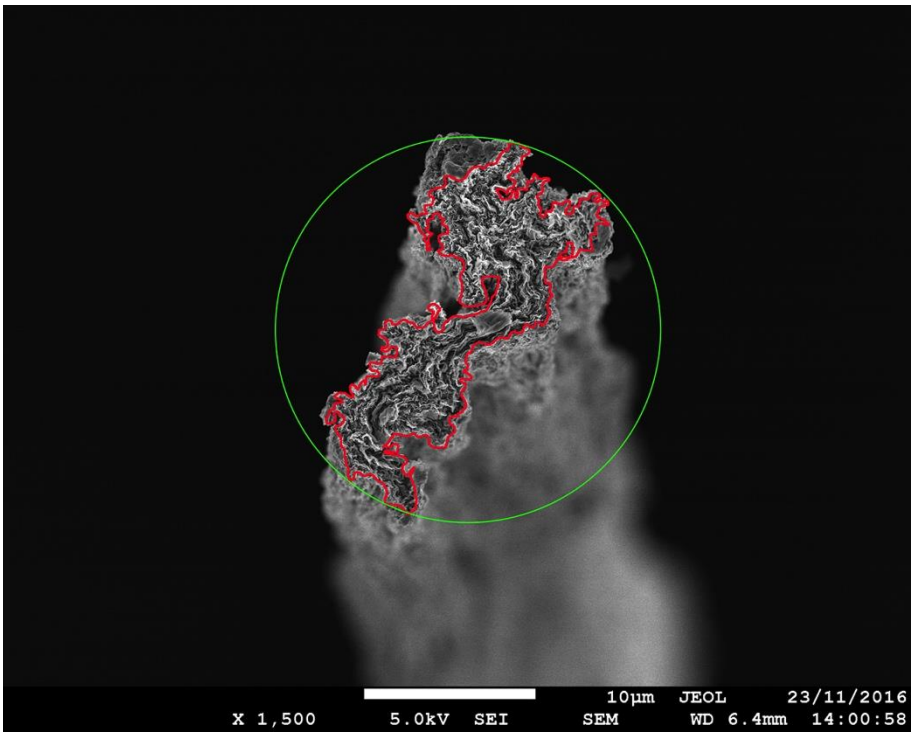

Figure S8. Representative SEM micrograph of the cross sections of a typical graphene fiber showing the reported diameter based on a circular cross section vs. actual area for the fiber. The diameter is calculated based on the area of a circle with a diameter equal to the longest width (green circle) of the irregular fiber, whereas, actual area is the exact measure of the area of an irregular fiber, as defined with the red line.

Electrochemical characterization

Cyclic voltammetry (CV) and electrochemical impedance spectroscopy (EIS) were performed with a CHI 660E electrochemical workstation (CH Instruments) in phosphate buffered saline (PBS, pH 7.4, Sigma-Aldrich) at room temperature. A three-electrode cell system was employed

with the test sample as working electrode, a platinum sheet as counter electrode, and Ag|AgCl as reference electrode. CVs were recorded between the voltages of -0.2 and 0.8 V at scan rates of 10-50000 mV/s. Each sample was tested for 3-5 cycles, and the cathodic charge storage capacity was calculated from the integration of current over time recorded in the last cycle at scan rate of 100 mV/s. Sweeps from -1.6 to 1.6 V were performed to determine the water window (e.g., threshold to electrolysis) of GF-Pt-PC electrodes, and the water oxidation and reduction potentials were determined when the sharp current peaks were detected. EIS was performed between frequencies of 1-10^4 Hz, and the specific impedance was calculated at 10^3 Hz.

Voltage transient measurement

Voltage transient measurement was performed on a two-electrodes set-up in PBS solution (pH 7.4, Sigma-Aldrich) at room temperature. A symmetric charge-balanced, cathodic first, biphasic current pulse with 100 µs width, 20 µs interphase open circuit potential and 2.78 ms short circuit at 250 Hz was generated by a digital stimulator DS800 and A365 Isolator units (World Precision Instruments). The voltage waveform across the active microelectrode in response to the applied current pulse was recorded with an e-corder system (eDAQ). The maximum negative polarization potential (E_{mc}) was calculated by subtracting the initial access voltage (V_a) from the total voltage transient. The charge injection capacity was determined when E_{mc} reached the water reduction limit from the following equation[3].

$$Q_{inj} = \frac{I_c \cdot t_c}{GSA}$$

Where Q_{inj} is the charge injection limit capacity, I_c is the current pulse applied, t_c is the pulse width, and GSA is the geometric surface area.

In-vivo implantation and neural recording

All procedures were performed in accordance to an animal use protocol 15-19 approved by the Institutional Animal Care and Use Committee at the University of Texas at Dallas on the 6th of January, 2017. A Long-Evans rat was selected for this study, while our target was within the motor cortex in the region associated with the control of the left forepaw. The animal was anesthetized using 2% isoflurane mixed in oxygen, which was followed by intraperitoneal administration of a cohort consisting of ketamine (65 mg/kg), xylazine (13.33 mg/kg), and acepromazine (1.5 mg/kg). The animal was mounted into a Kopf Model 900 small animal stereotaxic instrument (David Kopf Instruments, CA, United States). Dexamethasone (2 mg/kg) was administered subcutaneously over the shoulders to reduce the inflammatory response and was followed by the subcutaneous administration of 0.5% lidocaine (0.16 cc) directly under the scalp incision site. After exposing the skull, we created a 2.0 mm by 2.0 mm craniotomy with a center at our initial coordinates of implantation of 2.5 mm rostral and 2.5 mm lateral from bregma. The dura in the area was reflected using a dura pick followed by micro scissors to expose the surface of the cortex. The entire area was kept under liquid with frequent application of 7.4 pH sterile physiological phosphate buffered solution.

Five implants were selected for this proof-of-concept study. The first implant consisted of a bundle of four, 40 µm diameter microelectrodes composed of graphitic fibers coated with a thin layer of platinum and encapsulated with parylene-C insulation (GF-Pt-PC). The second microelectrode consisted of a single, 40 µm diameter graphitic fiber conductor encapsulated with parylene-C insulator (GF-PC). The third microelectrode was a single, 40 µm diameter GF-Pt-PC microelectrode. The final two microelectrodes consisted one GF-PC and one GF-Pt-PC with 20 µm diameters.

We loaded the bundle of four microelectrodes into a Model 2650 hydraulic micropositioner (David Kopf Instruments, CA, United States) into the microelectrode holder. The tips of the microfiber

wire bundle were lowered until they came into contact with the cortical surface at the implantation coordinates, the distance counter on the micropositioner was reset and the device was lowered into the motor cortex at a speed of 1000 µm/ s. If buckling of the wire began, the implantation was immediately stopped and the speed was reduced to 100 µm/ s. A sterile stainless steel hypodermic needle was inserted into the rat tail to serve as the counter electrode. The optimal implantation depth was 1500 µm.

Each acute recording was performed for at least 10 minutes using an OmniPlex D Neural Data Acquisition System (Plexon Inc., TX, United States). If no single neural units were acquired, we increased the depth of implantation by 200 µm and performed another recording. We continued to increase the depth of implantation until a successful recording with single units was acquired, or the wire implant reached a maximum depth of 2000 µm. After the recording, the microfiber wire/ bundle was explanted completely from the brain, the micropositioner was disinfected with isopropanol, and another wire was loaded in the micromanipulator. Each additional microfiber microelectrode was implanted at separate locations, with the second implant position located 200 µm rostral from the initial implant location. The third microelectrode was implanted 200 µm lateral from the second location, with the next at 200 µm caudal from the third location, and the last 100 µm from the third. Identical recording procedures were followed for all subsequent microelectrodes. After the investigation, the rat was euthanized using an overdose of 5% isoflurane vapor which was applied until breathing cessation occurred.

The wideband recordings obtained from OmniPlex D were further processed using Plexon's Offline Sorter software. The wideband signals were filtered using a 4^{th} order Butterworth filter with a cutoff located at 550 Hz and common-mode referencing was used to eliminate noise. The threshold to select single units was set to 3σ from peak height with the waveform duration of 1500 µs. Waveforms sorted from the threshold crossing were further evaluated using the software's

built-in Valley-Seeking algorithm. The noise envelope was obtained setting the threshold to ± 3σ of the original signal and removing the waveform segments 250 ms before and 750 ms after the threshold crossing. The average amplitude of the single unit waveforms was determined by the largest negative deflection from zero crossing. The reported signal-to-noise (SNR) ratio was calculated in decibels using the following formula:

$$SNR = 10log_{10}(\frac{A_{signal}}{A_{noise}})^2$$

References:
[1] R. Jalili, S. H. Aboutalebi, D. Esrafilzadeh, R. L. Shepherd, J. Chen, S. Aminorroaya-Yamini, K. Konstantinov, A. I. Minett, J. M. Razal, G. G. Wallace, Adv. Funct. Mater. 2013, 23, 5345.
[2] R. Jalili, J. M. Razal, P. C. Innis, G. G. Wallace, Adv. Funct. Mater. 2011, 21, 3363.
[3] S. F. Cogan, Annu. Rev. Biomed. Eng. 2008, 10, 275.